

Dynamics of two-dimensional coherent structures in nonlocal nonlinear media

A. I. Yakimenko^{1,2}, V. M. Lashkin¹, and O. O. Prikhodko²

¹*Institute for Nuclear Research, Prospect Nauki 47, Kiev 03680, Ukraine and*

²*Physical Department, Taras Shevchenko National University, Prospect Glushkova 2, Kiev 03680, Ukraine*

(Dated: June 6, 2018)

We study stability and dynamics of the single cylindrically symmetric solitary structures and dipolar solitonic molecules in spatially nonlocal media. The main properties of the solitons, vortex solitons, and dipolar solitons are investigated analytically and numerically. The vortices and higher-order solitons show the transverse symmetry-breaking azimuthal instability below some critical power. We find the threshold of the vortex soliton stabilization using the linear stability analysis and direct numerical simulations. The higher-order solitons, which have a central peak and one or more surrounding rings, are also demonstrated to be stabilized in nonlocal nonlinear media. Using direct numerical simulations, we find a class of radially asymmetric, dipole-like solitons and show that, at sufficiently high power, these structures are stable.

PACS numbers: 42.65.Sf, 42.65.Tg, 42.70.Df, 52.38.Hb

I. INTRODUCTION

The recent experimental observations of spatial solitons in nonlocal media such as nematic liquid crystals [1], lead glasses [2], renewed an interest to coherent structures in spatially nonlocal nonlinear media. In the spatially nonlocal media the nonlinear response depends on the wave packet intensity at some extensive spatial domain. Nonlocality is a key feature of many nonlinear media. It naturally appears in different physical systems such as plasmas [4, 5], Bose-Einstein condensates (BEC) [6], optical media [7], atomic nuclei [8], liquid crystals [1].

An important property of spatially nonlocal nonlinear response is that it prevents a catastrophic collapse which usually occurs in local self-focusing media when the power of the two- or three-dimensional wave packet exceeds some critical value. In particular, a rigorous proof of absence of collapse during the wave packet propagation described by the nonlocal nonlinear Schrödinger equation (NLSE) with sufficiently general symmetric real-valued response kernel has been presented in [7, 9]. In the absence of collapse, the competition between diffraction spreading and nonlinear self-action leads to formation of the stationary solitary wave structures - solitons and vortex solitons. Different types of two-dimensional self-trapped localized wave beams have been predicted and experimentally observed in various nonlinear media [10].

Fundamental solitons are the lowest-order localized structures with a single peak in the intensity distribution and transversely constant phase. A vortex is the structure with ring-like intensity distribution, with the dark hole at the center where the phase dislocation takes place: a phase circulation around the axis of propagation is equal to $2\pi m$. An integer m is referred to as topological charge. The important integral of motion associated with this type of solitary wave is the angular momentum, which can be expressed through the vortex power N and topological charge m as follows: $|\mathbf{M}| = mN$. Thus, vortices (or spinning solitons) are the localized structures with nonzero angular momentum. While the

fundamental solitons are robust in a collapse-free media, the spinning solitons may possess a strong azimuthal modulational instability [11]. As a result, the vortex decays into several ordinary solitons which fly off carrying out its energy and angular momentum. Though vortices can be stabilized in media with competing local nonlinearities [12, 13, 14, 15], it occurs only in the extreme regime when the higher-order contribution to the nonlinearity dominates. The recent investigations [16, 17] have shown that the different kinds of nonlocality of the nonlinear response can also suppress or completely eliminate the symmetry-breaking azimuthal instability for one-ring and double-ring single-charge ($m = 1$) vortex solitons. The recent experiments [2] have confirmed an existence of stable single-charge vortex solitons in the nonlocal media with thermal optical nonlinearity. The multicharge vortices ($m > 1$) are unstable in the media with thermal nonlocal nonlinearity, as was shown in Ref. [16] by linear stability analysis of small azimuthal perturbations and direct numerical modeling. On the other hand, the robust propagation of two-charge vortex ($m = 2$) solitons has been observed in the numerical simulations [17] for the model based on Gaussian-type kernel of the nonlocal media response function. We perform here the linear stability analysis for the model used in Ref. [17] and prove the possibility of stabilization of multicharge vortex solitons in the nonlocal nonlinear media.

The higher-bound solitons with field nodes (zero-crossing) have been first discovered in Ref. [26] for the local Kerr-type nonlinear media. The n th bound state has a central bright spot surrounded by n rings of varying size. In the local nonlinear media the higher-order solitons with zero angular momentum show the azimuthal instability [27, 28] similar to the instability of the vortex solitons. The rings which surround the central peak possess an azimuthal instability. As a result, the higher-bound structures decay into several fundamental solitons. We reveal here that nonspinning higher-order solitons can be stabilized in the nonlocal medium.

Another important feature of nonlocal nonlinear me-

dia is the possibility of existence of composite soliton structures. A composite soliton structure, or a multi-soliton complex is a self-localized state which is a nonlinear superposition of several fundamental solitons [3, 18]. Multi-soliton structures in nonlocal media were considered first in Refs. [19, 20], and they have recently received renewed interest [21, 22, 23]. In particular, one-dimensional (1D) nonlocal model suggested in Ref. [4] was studied in Ref. [23] and it was shown that dipole-, triple-, and quadrupole-mode solitons can be made stable. Very recently [24] two-dimensional (2D) rotating dipole structures were considered in the framework of an approximate variational approach. In this paper, using direct 2D simulations, we find numerically a class of radially asymmetric two-dimensional dipole-mode soliton solutions and show that, at sufficiently high input power, these solutions are stable.

The aim of this paper is to study general properties and to carry out the stability analysis of single solitons (both fundamental and higher-bound states), vortex solitons, and composite dipole-like solitons in the strongly nonlocal media.

The paper is organized as follows. In Sec. II we formulate a model and present basic equations. The stability analysis based on the variational approach and numerical simulations for single solitary structures is performed in Sec. III, and then, in Sec. IV, we consider the multisoliton dipole-like structures. The conclusions are given in Sec. V.

II. BASIC EQUATIONS

We consider propagation of the electric-field envelope $\Psi(x, y, z)$ described by the paraxial wave equation:

$$i\frac{\partial\Psi}{\partial z} + \Delta_{\perp}\Psi + \Theta\Psi = 0, \quad (1)$$

where z is the direction of beam propagation, Θ represents the nonlinear response of the media.

Equation (1) conserves the following integrals of motion: (i) number of quanta (“energy” or “beam power”):

$$N = \int |\Psi|^2 d^2\mathbf{r}, \quad (2)$$

(ii) momentum:

$$\mathbf{I}_{\perp} = -\frac{i}{2} \int (\Psi^* \nabla_{\perp} \Psi - \Psi \nabla_{\perp} \Psi^*) d^2\mathbf{r},$$

(iii) angular momentum:

$$\mathbf{M} = -\frac{i}{2} \int [\mathbf{r} \times (\Psi^* \nabla_{\perp} \Psi - \Psi \nabla_{\perp} \Psi^*)] d^2\mathbf{r},$$

(iv) Hamiltonian:

$$H = \int \left\{ |\nabla_{\perp} \Psi|^2 - \frac{1}{2} \Theta |\Psi|^2 \right\} d^2\mathbf{r}.$$

The nonlocal nonlinear media response function can be taken as follows:

$$\Theta(\vec{r}) = \int R(|\vec{r} - \vec{r}_1|) |\Psi(\vec{r}_1)|^2 d^2\mathbf{r}_1. \quad (3)$$

The shape of the kernel $R(r)$ is determined by the type of the nonlocal interaction in media and can be rather complicated [6, 16]. However, there are general properties valid for all nonlocal media response functions. The nonlinear term tends to the local Kerr-type nonlinearity: $\Theta \rightarrow |\Psi|^2$ when the spatial scale of the wave packet intensity distribution $|\Psi|^2$ is much wider than the effective width of the potential $R(r)$. In the opposite case of the strongly nonlocal regime, the response function can be estimated as follows: $\Theta(r) = N \{ R(0) + \frac{1}{2} \Delta R(0) r^2 \}$. In the latter case, the highly-nonlocal NLSE (1) with a sufficiently regular kernel $R(r)$ is mathematically identical to the linear Schrödinger equation with harmonic oscillator potential, as was pointed out in Ref. [29].

We consider in this paper the nonlocal response function kernel modeled by the Gaussian shape kernel:

$$R(|\vec{r} - \vec{r}_1|) = \frac{\alpha^2}{\pi} e^{-\alpha^2 |\vec{r} - \vec{r}_1|^2}, \quad (4)$$

where α is the nonlocality parameter. Keeping the main features of nonlocal media this model allows a very accurate and simple analytical treatment.

III. SINGLE SOLITARY STRUCTURES

In this section, we study single solitons (both fundamental and higher-bound states) and vortex solitons. We look for the stationary solutions of the Eq. (1) in the form:

$$\Psi(x, y, z) = \psi(r) e^{im\varphi + i\Lambda z}, \quad (5)$$

where φ and $r = \sqrt{x^2 + y^2}$ are the azimuthal angle and the radial coordinate, respectively, and Λ is the beam propagation constant. Such solutions describe either the soliton, when $m = 0$, or the vortex soliton with the topological charge m , when $m \neq 0$. The function $\psi(r)$ obeys the integro-differential equation:

$$-\Lambda\psi + \Delta_r^{(m)}\psi + \theta\psi = 0. \quad (6)$$

The boundary conditions for the localized solutions are: $\psi(\infty) = 0$ and $(d\psi/dr)_{r=0} = 0$ for solitons, $\psi(0) = 0$ for vortices. For the stationary solution (5) it is easy to rewrite the response function in the form:

$$\theta(r) = 2\alpha^2 \int_0^{+\infty} e^{-\alpha^2(r-r_1)^2} \mathcal{I}_0(2\alpha^2 r r_1) |\psi(r_1)|^2 r_1 dr_1, \quad (7)$$

where $\mathcal{I}_\nu(x) = e^{-x} I_\nu(x)$ is the exponentially scaled modified Bessel function.

In the next subsection we start our considerations on the single cylindrically symmetric solitary structures with the analytical analysis based on the variational approach.

A. Variational approach

As known [29], the nonlocal NLSE turns to the linear Schrödinger equation with harmonic oscillator potential in the highly-nonlocal limit, when the spatial scale of the response function is much wider than the wave packet localization region. Since the Laguerre-Gauss modes are the exact eigenstates for the two-dimensional linear oscillator, the variational method with the trial function of the form

$$\Psi(x, y, z) = h(z) \xi^m L_n^{(m)}(\xi^2) e^{-\frac{1}{2}\xi^2\{1+i\tilde{b}(z)\}+im\varphi+i\Phi(z)}, \quad (8)$$

is expected to give an accurate description of all eigenmodes, especially in the highly nonlocal regime. Here $L_n^{(m)}(x)$ is the generalized Laguerre polynomial, n is the number of nodes of the radial profile, and m is the topological charge, $\xi = r/a(z)$, where $a(z)$ is the first variational parameter that characterizes a radius of solitary structure: $a^2 = \langle r^2 \rangle (2n + m + 1)^{-1}$, where $\langle r^2 \rangle = N^{-1} \langle \Psi | r^2 | \Psi \rangle$ is the mean-square radius. The second variational parameter $\tilde{b}(z)$ is the phase curvature. The amplitude $h(z)$ can be readily found from the relation $h(z)a(z) = \sqrt{\frac{n!N}{\pi(n+m)!}}$, which is obtained from normalization condition (2).

We start our considerations with the lower-order nodeless states ($n = 0$). The nonlinear response function in the framework of variational approach is given by expression:

$$\Theta(r) = h^2 q e^{-q\xi^2} m! (1 - q)^m L_m(q^2 \xi^2 / (q - 1)),$$

where $q = \alpha^2 a^2 / (1 + \alpha^2 a^2)$, $L_m(x) = L_m^{(0)}(x)$ is Laguerre polynomial of m -th order. Note, if $a^2 \alpha^2 \gg 1$, then $q \rightarrow 1$, and one obtains $\Theta \rightarrow |\Psi|^2$, as it should be in the local limit.

In accordance with the variational procedure, we construct the Lagrangian density

$$\ell = \frac{i}{2} \left(\Psi \frac{\partial \Psi^*}{\partial z} - \Psi^* \frac{\partial \Psi}{\partial z} \right) + |\nabla_{\perp} \Psi|^2 - \frac{1}{2} \Theta |\Psi|^2$$

and the Lagrangian

$$\mathcal{L} = \int \ell \, d^2 \mathbf{r} = N \dot{\Phi} + \frac{(m+1)}{2} N \left[b \dot{a} - \dot{b} a \right] + H,$$

where $b = \tilde{b}/a$, H is the Hamiltonian:

$$H = N \left\{ (m+1) (1/a^2 + b^2) - \frac{N h_m(a)}{2\pi a^2} \right\},$$

where $h_m(a) = q (1 - q)^m (1 + q)^{-m-1} P_m\left(\frac{1+q^2}{1-q^2}\right)$, $P_m(x)$ is the Legendre polynomial of the m -th order.

The first two dynamical equations can be written in the canonical form:

$$\frac{N(m+1)}{2} \frac{da}{dz} = -\frac{\partial H}{\partial b}, \quad \frac{N(m+1)}{2} \frac{db}{dz} = \frac{\partial H}{\partial a} \quad (9)$$

and the third one is the following: $dN/dz = 0$ which means that the number of quanta is the integral of motion. The soliton or vortex soliton corresponds to the stationary point of the Hamiltonian: $\partial H/\partial b = 0$, $\partial H/\partial a = 0$. The first condition yields $b_0 = 0$. From the second equation one can find the width a_0 as the function of the number of quanta N . It is easy to verify that vortex or soliton can exist only above the threshold value for number of quanta: $N > N_{cr} = 4^{m+1} \pi (m+1) (m!)^2 / (2m)!$. Using the similar procedure we have considered the non-spinning ($m = 0$) higher-bound states with one ($n = 1$) and two nodes ($n = 2$). The thresholds for an existence of the higher bound states are as follows: $N_{cr} = 24\pi$ for $n = 1$ and $N_{cr} = 640\pi/11$ for $n = 2$.

The described variational procedure provides the possibility for analysis of the stationary radially-symmetric coherent structures. The results of the variational analysis are given in Fig. 1 (a) for fundamental solitons and vortex solitons, and in Fig. 2 for higher-order solitons.

Moreover, using the set (9) it is possible to study the radially-symmetric dynamics of the localized wavepackets propagating in z -direction. Let us investigate, for example, the evolution of a slightly perturbed stationary soliton solution. It can easily be shown that the small deviation of the soliton width $\delta = a - a_0$ from the stationary value a_0 obeys the equation $\ddot{\delta} + \omega^2 \delta = 0$, where $\omega^2 = 8N^{-1}(\partial^2 H/\partial a^2)_{a_0, b_0}$. Therefore, the soliton being radially perturbed exhibits the oscillations with the frequency $\omega = 8\alpha^2 \pi^{-1/2} [1 - \sqrt{N_{cr}/N}]^{3/2}$, where $N_{cr} = 4\pi$ is the threshold for soliton existence.

However, one cannot study the stability of stationary solutions with respect to symmetry-breaking azimuthal perturbations in the framework of a variational approach with a radially symmetric trial function. Stability conditions of steady-state solutions, regarding small general 2D perturbations, will be obtained by a linear stability analysis in the next subsection.

B. Numerical modeling

The boundary problem (6) is equivalent to the integral equation:

$$\psi(r) = \int_0^{+\infty} \theta(\eta) \psi(\eta) G_m(\eta, r; \sqrt{\Lambda}) \eta \, d\eta, \quad (10)$$

where θ is given by Eq. (7),

$$G_m(\xi_1, \xi_2; a) = \begin{cases} K_m(a\xi_2) I_m(a\xi_1), & 0 \leq \xi_1 < \xi_2, \\ I_m(a\xi_2) K_m(a\xi_1), & \xi_2 < \xi_1 < +\infty, \end{cases} \quad (11)$$

where I_m and K_m are the modified Bessel functions of the first and second kind, respectively. We have solved the nonlinear integral equation (10) using stabilized iterative method [25]. For numerical modeling it is useful to perform the rescaling transformation of the form: $r' = \alpha r$, $\psi' = \psi/\alpha$, $\theta' = \theta/\alpha^2$, $z' = z\alpha^2$. Such transformation reduces the number of parameters to one dimensionless

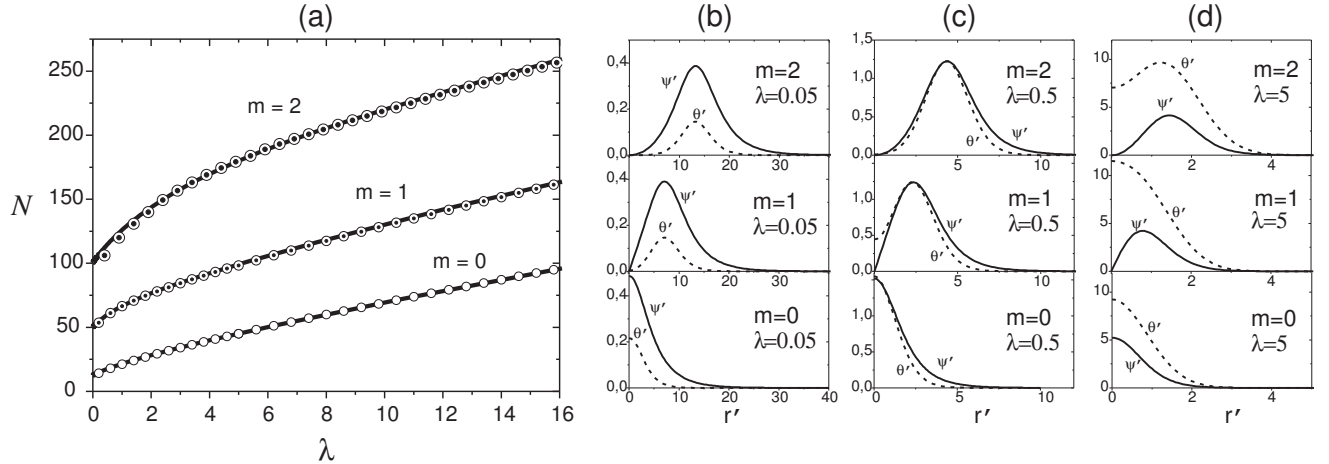


FIG. 1: (a) Number of quanta N vs parameter $\lambda = \Lambda/\alpha^2$ for solitons ($n = 0, m = 0$) and vortex solitons ($n = 0, m = 1, 2$) (solid curves for variational and circles for numerical results). Numerically found profiles for (b) $\lambda = 0.05$; (c) $\lambda = 0.5$; (d) $\lambda = 5$. Solid curves for $\psi'(r') = \psi/\alpha$ dashed curves for $\theta'(r') = \theta/\alpha^2$; the scaled coordinates $r' = \alpha r$ are used.

parameter $\lambda = \Lambda/\alpha^2$. Figure 1 (b)-(d) shows several examples of the numerical solution of the (6) at different values of the parameter λ . Note, that the nonlocal limit $\alpha^2 \ll \Lambda$ corresponds to the large values of the parameter λ and, as seen from Fig. 1 (a), to the large values of the beam power N .

Let us investigate the stability of the steady-states with respect to small azimuthal perturbations. Expanding the nonstationary solution in vicinity of a steady-state:

$$\Psi(r, z) = \{\psi(r) + \delta\psi_+ + \delta\psi_-^*\} e^{i\Lambda z + i\Lambda\varphi},$$

where $\delta\psi_{\pm}(r, \varphi, z) = \varepsilon_{\pm}(r)e^{i\omega z + iL\varphi}$, and linearizing the dynamical Eq. (1) one can obtain the eigenvalue problem for ω of the form:

$$\begin{pmatrix} \hat{Q}_{m+L} + \hat{g}_L & \hat{g}_L \\ -\hat{g}_L & -\hat{Q}_{m-L} - \hat{g}_L \end{pmatrix} \vec{\varepsilon} = \omega \vec{\varepsilon}, \quad (12)$$

where $\vec{\varepsilon} = (\varepsilon_+, \varepsilon_-)$, and $|\text{Im}\omega|$ determines the growth rate of an unstable mode,

$$\hat{Q}_{m\pm L} \varepsilon_{\pm} = \left\{ -\Lambda + \Delta_r^{(m\pm L)} + \theta(r) \right\} \varepsilon_{\pm},$$

$$\hat{g}_L \varepsilon_{\pm} = 2\alpha^2 \psi(r) \int_0^\infty \psi(\xi) \chi(r, \xi) \varepsilon_{\pm}(\xi) d\xi,$$

$\chi(r, \xi) = \xi e^{-\alpha^2(r-\xi)^2} \mathcal{I}_L(2\alpha^2 r \xi)$. The unperturbed radial profile $\psi(r)$ is taken to be real without loss of generality. We have used the Hankel spectral transformation and reduced the integro-differential eigenvalue problem (12) to the linear algebraic one. Figure 3 (a) shows the maximum growth rate for one-charge ($m = 1$) vortex solitons. It is seen that only modes having $L = 1, 2, 3$ can be unstable. Modulational instability is strongly suppressed in a highly-nonlocal regime: the growth rates vanish at some finite values of parameter λ . The mode with azimuthal

number $L = 2$ corresponds to the largest growth rates with widest instability region: all growth rates are equal to zero at $\lambda > \lambda_{cr} \approx 9.1$. Similar analysis has been performed for multi-charge vortices (with $m = 2, \dots, 5$). Figure 3 (b) depicts the growth rates for two-charge ($m = 2$) vortex solitons. Note that the modulation instability is eliminated for $\lambda > \lambda_{th} \approx 23.8$. Thus, in the media with the nonlocal response of the form (4) the multi-charge vortices can be stabilized. Note that vortex solitons with $m > 1$ are found [16] to be unstable in the media with thermal nonlocal nonlinearity. Therefore, the dynamical properties of the vortex structures can be significantly affected by specific type of the nonlocal interaction.

The results of linear analysis have been confirmed by extensive series of numerical simulations of dynamics of perturbed stationary solutions. We have performed the split-step Fourier transform method to solve the dynamical Eq. (1) with the response function Eq. (3). The nonlocal nonlinear term has been calculated in the spectral domain, since it has the form of the convolution of the intensity distribution $|\Psi(\vec{r})|^2$ with the function $R(|\vec{r}|)$. We have used the numerically found stationary vortex solitons and variational profiles for the higher-order solitons as the initial conditions. Different kinds of the perturbations such as random noise, radially-symmetric and azimuthal periodic perturbations have been applied in the numerical experiments. The conclusions of the linear stability analysis are found to be in a good agreement with our simulations: the vortex solitons become stable above some critical power which is close to the one predicted by linear stability analysis.

Figure 4 (a) illustrates the unstable evolution of the single-charge vortex soliton. In the stable region, when $\lambda > \lambda_{cr}$, vortices survive even being strongly perturbed. The mean-square radius and intensity of the vortex oscillate, but the vortex ring shows the robust propagation over vast distances (thousands of diffraction lengths) for

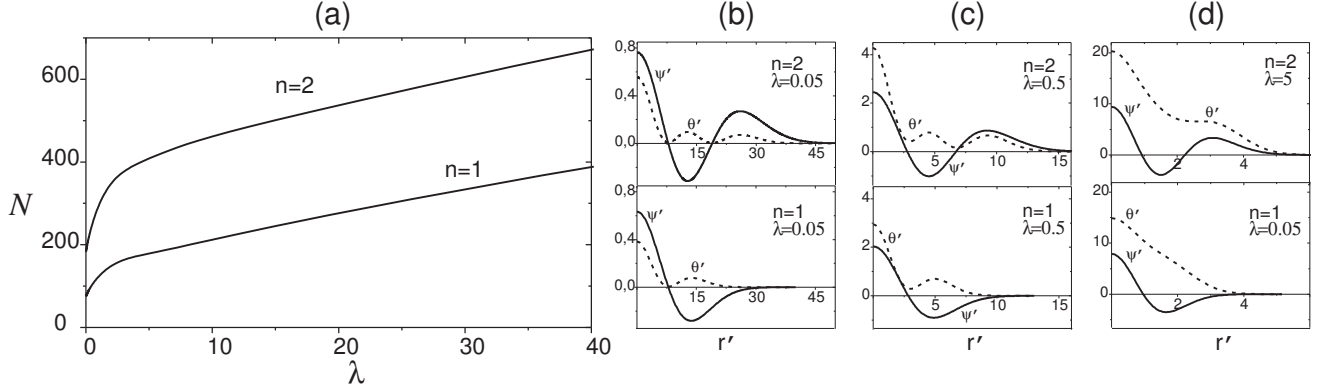


FIG. 2: (a) Number of quanta N vs parameter $\lambda = \Lambda/\alpha^2$ for higher-order solitons ($m = 0$, $n = 1, 2$). Radial profiles for (b) $\lambda = 0.05$; (c) $\lambda = 0.5$; (d) $\lambda = 5$. Solid curves for ψ' dashed curves for θ' .

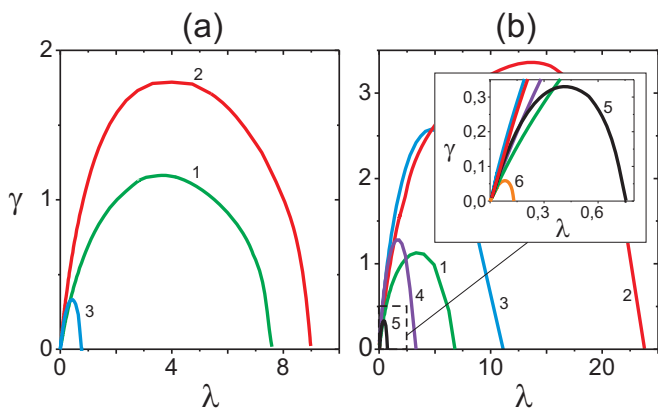


FIG. 3: (Color online) The scaled growth rate $\gamma = \text{Im}\omega/\alpha^2$ of linear perturbation modes vs the parameter $\lambda = \Lambda/\alpha^2$ for the vortices with (a) $m = 1$ and (b) $m = 2$, the inset depicts the growth rates of the high- L modes in more details. The numbers near the curves stand for the azimuthal mode numbers L .

the hundreds of the effective periods of the oscillation. The higher-order solitons exhibit similar decay in weakly nonlocal regime. However, when beam power increases, an interesting dynamics with revivals has been observed [see Fig. 4 (b)]. Initially field envelope decays into several filaments, but then it recurs at larger propagation distances. With further increasing of the power, a higher-order soliton occurs to be stabilized: it shows the robust propagation without breakup during the hundreds of effective oscillation periods.

IV. STABLE BISOLITON MOLECULES

In this section, we present and study localized asymmetric dipole-like solutions. We look for stationary solutions of Eq. (1) in the form $\Psi(x, y, z) = \psi(x, y) \exp(i\Lambda z)$,

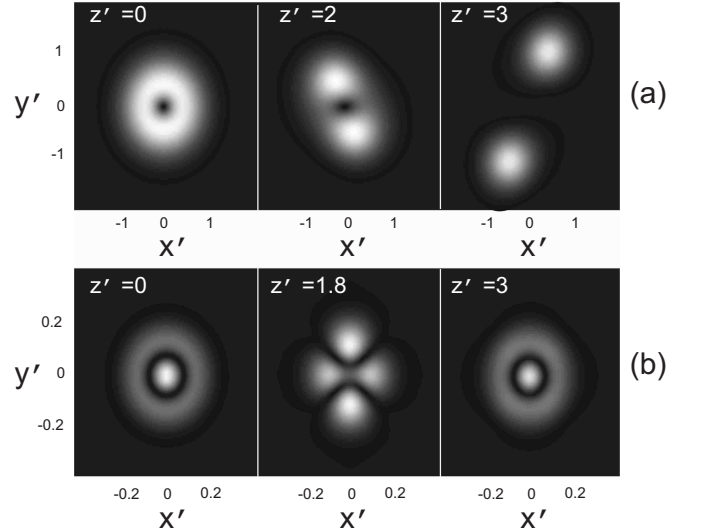


FIG. 4: Snapshots of $|\Psi'(x', y')|$ for different z' . (a) Example of unstable evolution of single-charge ($m = 1$, $n = 0$) vortex soliton with $\lambda = 4$. (b) Dynamics with revival of the non-spinning ($m = 0$) one-node ($n = 1$) soliton at $\lambda = 35$.

so that $\psi(x, y)$ obeys the equation

$$-\Lambda\psi + \Delta_{\perp}\psi + \theta\psi = 0, \quad (13)$$

where

$$\theta = \frac{\alpha^2}{\pi} \int e^{-\alpha^2[(x-x_1)^2+(y-y_1)^2]} \psi^2(x_1, y_1) d^2\mathbf{r}_1. \quad (14)$$

and we do not assume the radial symmetry of $\psi(x, y)$. Unlike the NLSE with local cubic nonlinearity, equation (13) with the nonlocal nonlinear media response θ given by Eq. (14) has two characteristic transverse scales: the internal scale $\Lambda^{1/2}$ (in the NLS this scale determines the characteristic size of the soliton) and the "external" scale α which is the measure of nonlocality. Under this, the characteristic size of the self-consistent potential well in Eq. (1) can significantly differ from $\Lambda^{-1/2}$ and, thus, the

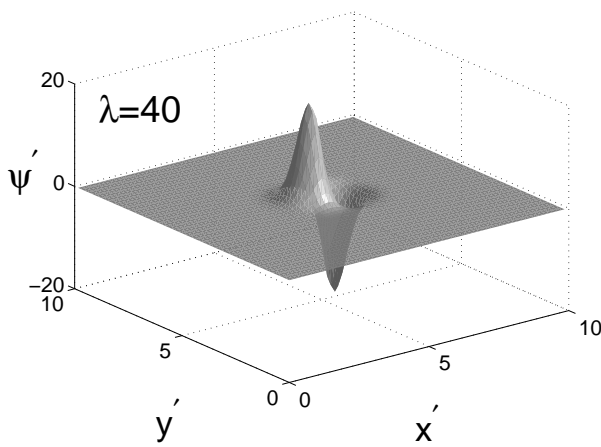


FIG. 5: The dipole solution $\psi' = \psi/\alpha$ for $\lambda \equiv \Lambda/\alpha^2 = 40$; the scaled coordinates $x' = \alpha x$ and $y' = \alpha y$ are used.

existence of composite soliton structures becomes possible. In this paper we restrict ourselves to dipole-like localized solutions. Results concerning the tripolar and higher radially asymmetric soliton modes will be published elsewhere.

As above, we use the scaled variables ψ' , z' , $x' = \alpha x$, and $y' = \alpha y$. Imposing periodic boundary conditions on Cartesian grid and choosing an appropriate initial guess, one can find numerically dipole-type localized solutions by using the relaxation technique similar to one described in Ref. [25]. An example of such dipole solution is presented in Fig. 5. The dipole consists of two out-of-phase monopoles. The characteristic width of the monopoles in the dipole and the "distance" between them decrease with increasing the parameter $\lambda = \Lambda/\alpha^2$.

We next addressed the stability of these dipole solutions and study the evolution (propagation) of the dipoles in the presence of small initial perturbations. We have undertaken extensive numerical modeling of Eqs. (1), (3) and (4) initialized with our computed dipole-type solutions with added gaussian noise. Spatial discretization was based on the pseudospectral method and "temporal" z -discretization included the split-step scheme. The numerical simulations clearly show that the dipoles with $\lambda > \lambda_{th}$, where $\lambda_{th} \approx 21$ is the threshold value, are stable with respect to small initial noisy perturbations up to the maximum propagation distances used (of the order of $z' = 3000$). The stable propagation of the dipole is illustrated in Figs. 6(a), (b). Additionally, the stable dynamics was monitored by plotting the z' dependencies of the averaged intensity $\int |\psi|^4 d\mathbf{r}/N$ and mean-square radius $\int r^2 |\psi|^2 d\mathbf{r}/N$. For stable propagation, these quantities undergo small oscillations near the equilibrium values. Note, that dipoles with sufficiently large (compared to λ_{th}) values of λ survive over huge distances (many thousands of diffraction lengths) in the presence

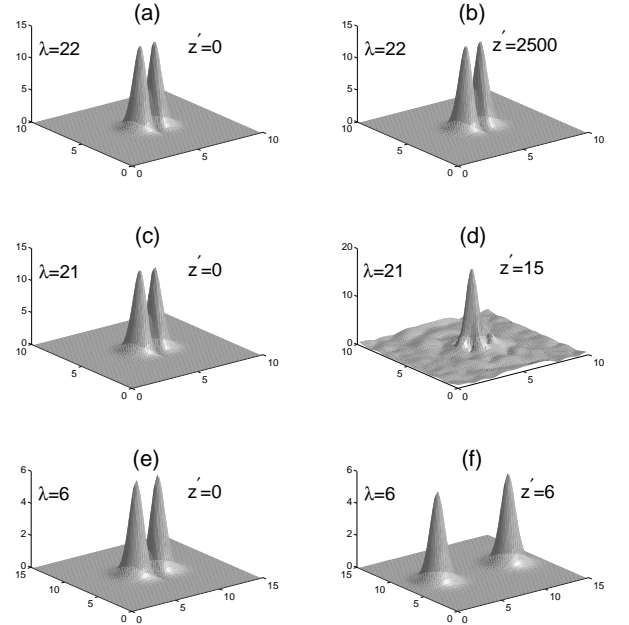


FIG. 6: Snapshots of $|\psi'(x', y')|$ for dipole propagation in the presence of small random perturbation for different $\lambda = \Lambda/\alpha^2$, shown in the scaled $(x' = \alpha x, y' = \alpha y)$ plane, at different moments z : (a), (b) - stable propagation; (c), (d) - destruction of the original dipole; (e), (f) - decay into two solitons.

of quite significant perturbations. We performed a series of runs for $\lambda > 200$ in the presence of strong initial noise. The initial condition was taken in the form $\psi'(x', y')[1 + \varepsilon f(x', y')]$, where $\psi'(x', y')$ is the numerically calculated exact dipole solution, $f(x', y')$ is the white gaussian noise with variance $\sigma^2 = 1$ and the parameter of perturbation $\varepsilon = 0.1 \div 0.3$. Snapshots of $|\psi'(x', y')|$ at different z' for the case $\lambda = 400$ and $\varepsilon = 0.12$ are presented in Fig. 7. One can see that the dipole turns out to be extremely robust - even at $z' = 2000$ one can not detect any substantial distortion of the dipole shape. The dipoles, however, become unstable (even if the initial noise is very small) if $\lambda < \lambda_{th}$. The typical decay of the unstable dipole near the threshold value of the rescaled propagation constant is shown in Figs. 6(c), (d).

The situation, however, changes below $\lambda_{cr} \approx 7.6$. Under this, the dipole splits in two monopoles which move in the opposite directions without changing their shape, i. e. the monopoles just go away at infinity. In Fig. 8 we plot the dipole energy N_{dip} and the doubled energy $2N_{mon}$, where N_{mon} is the energy of the monopole soliton solution of Eq. (13), calculated numerically, versus the propagation constant Λ . One can see that the bound energy $\delta N = N_{dip} - 2N_{mon}$ in the dipole tends to almost zero as λ approaches $\lambda_{cr} = 7.6$. This explains why the dipole with $\lambda \leq \lambda_{cr}$ can be easily (i. e. under the action of extremely small initial perturbations) split into two monopole-type solitons.

The results of the numerical simulation can be illus-

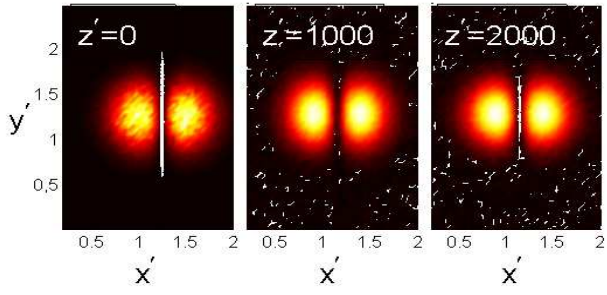


FIG. 7: (Color online) Evolution of the dipole solution with $\lambda = 400$ in the presence of strong initial random perturbation; the scaled variables $x' = \alpha x, y' = \alpha y$ and $z' = \alpha^2 z$ are used.

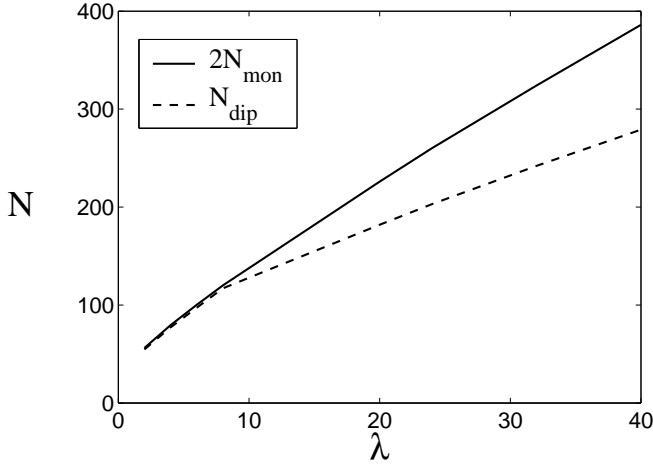


FIG. 8: The doubled energy of the soliton (monopole) $2N_{mon}$ (solid line) and the energy of the dipole N_{dip} (dashed line) v. s. the parameter $\lambda = \Lambda/\alpha^2$.

trated through the variational analysis. Equation (13) (in the scaled variables) is the Euler-Lagrange equation for the Lagrangian

$$\mathcal{L} = \int \left[|\nabla \psi'|^2 - \frac{1}{2} \theta \psi'^2 + \lambda \psi'^2 \right] d^2 \mathbf{r}. \quad (15)$$

Taking a trial function in the form

$$\psi' = A e^{-\beta^2[(x' - d/2)^2 + y'^2]} - A e^{-\beta^2[(x' + d/2)^2 + y'^2]}, \quad (16)$$

where A, β and d are unknown parameters to be determined by the variational procedure, and substituting it into Eq. (15), we get

$$\mathcal{L} = \pi A^2 \left(2c_1 - \frac{A^2}{4} c_2 + \lambda c_3 \right), \quad (17)$$

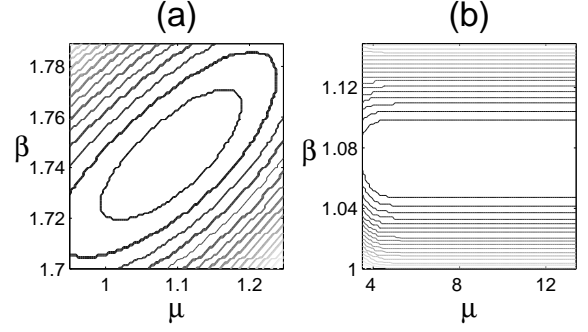


FIG. 9: Contour maps of the function $\mathcal{L}(\beta, \mu)$: (a) $\lambda = 40$; (b) $\lambda = 7.6$

where

$$c_1 = 1 - (1 - \mu^2/2)e^{-\mu^2/2}, \quad (18)$$

$$c_2 = \frac{1}{\beta^2(1 + \beta^2)} [1 + 2e^{-\mu^2} + e^{-\mu^2/(1 + \beta^2)} - 4e^{-(3 + 2\beta^2)\mu^2/4(1 + \beta^2)}], \quad (19)$$

$$c_3 = \frac{1}{\beta^2} \left(1 - e^{-\mu^2/2} \right), \quad (20)$$

and, instead of d , we have introduced the variational parameter $\mu = \beta d$. The optimum A satisfies the equation $\partial \mathcal{L} / \partial A = 0$ which yields

$$A^2 = \frac{4c_1 + 2\lambda c_3}{c_2}. \quad (21)$$

The Lagrangian Eq. (17), where A^2 is defined by Eq. (21), depends only on two unknown variational parameters β and μ (or, equivalently, β and d) and can be easily analyzed numerically. The topography of the function $\mathcal{L}(\beta, \mu)$ depends on the rescaled propagation constant $\lambda = \Lambda/\alpha^2$. There is the only minimum if $\lambda > \lambda_{cr}$, where λ_{cr} is some critical value. The contours (level lines) of the function $\mathcal{L}(\beta, \mu)$ for $\lambda = 40$ are shown (in the vicinity of the minimum) in Fig. 9 (a). In this case the minimum takes place at $\beta = 1.74$ and $\mu = 1.1$, and corresponds to the dipole solution presented in Fig. 5. The amplitude of the approximate analytical solution A calculated from Eq. (21) and the parameters β and μ are in agreement with corresponding values estimated from the exact numerical solution - the comparison of the variational analysis and the direct numerical simulation is presented in Fig. 10 (a). The dependence of the width of the monopoles β^{-1} in the dipole and the "distance" d between them on λ is shown in Fig. 10 (b). The topography of the function $\mathcal{L}(\beta, \mu)$ in the vicinity of the minimum represents a long narrow valley oriented at some angle to the μ -axis. Under this, the depth of the valley and the angle to the μ -axis decreases with decreasing λ . A similar situation holds for all $\lambda > \lambda_{cr}$ and we found $\lambda_{cr} \approx 7.6$. The picture changes sharply at $\lambda = \lambda_{cr}$. The local minimum disappears, the saddle point arises, and

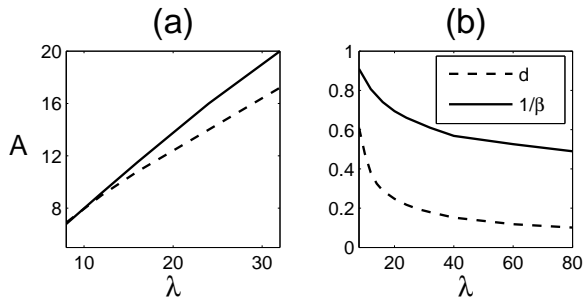


FIG. 10: (a) The dependence of the dipole amplitude A on λ : solid curve - variational analysis; dashed curve - direct numerical simulation. (b) Dipole distance d and the width β^{-1} v. s. λ (variational analysis)

this corresponds to the unstable dipole decaying into two monopoles. The contours of the function $\mathcal{L}(\beta, \mu)$ in this case (for $\lambda = 7.6$) are shown in Fig. 9 (b). The found critical value $\lambda_{cr} = 7.6$ is in perfect agreement with the results of direct numerical simulation (see Fig. 8(b)).

V. SUMMARY AND CONCLUSIONS

We have investigated the main properties and stability of the stationary two-dimensional localized solitary structures in the nonlocal nonlinear media. We have studied both fundamental and higher-order solitons; one-charge and multi-charge vortex solitons with nonzero angular momentum; dipolar multisolitons. While the fundamen-

tal soliton is always stable, the vortex solitons possess a strong azimuthal instability which is eliminated only in the strongly nonlocal regime. We have performed the linear stability analysis and direct numerical simulations to investigate the stability of vortices with arbitrary topological charge. We have found the edge of the modulational instability and predicted the threshold for the beam power of the robust vortex soliton. We prove that in contrast to the nonlocal media with thermal nonlinearity, the nonlinear response with the Gaussian-type kernel can sustain not only single-charge but also multi-charge vortices. We have investigated nonlocal higher-order nonspinning solitons which are the structures with the intensity distribution in the form of a bright spot surrounded by the bright rings. We theoretically predict an existence of stabilized higher-order nonspinning solitons in the nonlocal media. Finally, we have found stationary dipole-like multisolitons which are the bound states of the out-of-phase fundamental solitons. We have simulated numerically the dynamics of the multisolitons in the presence of initial noise and performed simple variational analysis. It turns out that multisolitons are extremely robust at sufficiently high input power in a highly nonlocal media. Therefore, these predictions open the prospects for the experimental observations of a wide class of stable coherent structures in various nonlocal nonlinear media.

Acknowledgments

We are grateful to Yu.A. Zaliznyak for discussions and comments about this paper.

[1] C. Conti, M. Peccianti, and G. Assanto, Phys. Rev. Lett. **92**, 113902 (2004).
[2] C. Rotschild, O. Cohen, O. Manela, M. Segev, and T. Carmon, Phys. Rev. Lett. **95**, 213904 (2005).
[3] N. Akhmediev and A. Ankiewicz, Chaos **10**, 600 (2000).
[4] A.G. Litvak, V.A. Mironov, G.M. Fraiman, and A.D. Yudakovskii, Sov. J. Plasma Phys. **1**, 60 (1975).
[5] T.A. Davydova, A.I. Fishchuk Ukrainian Journal of Physics Vol.40. p. 487, (1995)
[6] P. Pedri and L. Santos Phys. Rev. Lett. **95**, 200404 (2005)
[7] W. Królikowski, O. Bang, N.I. Nikolov, D. Neshev, J. Wyller, J.J. Rasmussen, and D. Edmundson, J. Opt. B **6**, 288 (2004).
[8] I.V. Simenog Teor. Mat. Fiz. **30**, pp 408-414 (1977)
[9] S.K. Turitsyn Theoretical and mathematical physics Vol.64, p.226 (1985)
[10] See, e.g., Yu.S. Kivshar and G. Agrawal, *Optical Solitons: From Fibers to Photonic Crystals* (Academic Press, San Diego, 2003) and references therein.
[11] D.V. Skryabin and W.J. Firth Phys. Rev. E, Vol.58, p.3916 (1998).
[12] M. Quiroga-Teixeiro and H. Michinel, J. Opt. Soc. Am. B **14**, 2004 (1997).
[13] V.L. Berezhiani, V. Skarka, and N.B. Aleksic Phys. Rev. E, Vol.64 057601 (2001)
[14] I. Towers, A.V. Buryak, R. A. Sammut, B. A. Malomed, L.-C. Crasovan, and D. Mihalache, Phys. Lett. A **288**, 292 (2001); Phys. Rev. E **63**, 055601 (2001)
[15] T.A. Davydova, A.I. Yakimenko, and Yu.A. Zaliznyak, Phys. Rev. E **67**, 026402 (2003)
[16] A.I. Yakimenko, Yu.A. Zaliznyak, and Yu. Kivshar Phys. Rev. E **71**, 065603 (2005)
[17] D. Briedis et al., Opt. Express 13, 435 (2005)
[18] A. S. Desyatnikov, A. A. Sukhorukov, and Yu. S. Kivshar, Phys. Rev. Lett. **95**, 203904 (2005).
[19] I. A. Kolchugina, V. A. Mironov, and A. M. Sergeev, Pis'ma Zh. Eksp. Teor. Fiz. **31**, 333 (1980) [JETP Lett. **31**, 304 (1980)].
[20] V. A. Mironov, A. M. Sergeev, and E. M. Sher, Dokl. Akad. Nauk SSSR **260**, 325 (1981) [Sov. Phys. Dokl. **26**, 861 (1981)].
[21] N. I. Nikolov, D. Neshev, O. Bang, and W. Królikowski, O. Bang, J. J. Rasmussen, and P. L. Christiansen, Phys. Rev. E **68**, 036614 (2003).
[22] N. I. Nikolov, D. Neshev, W. Królikowski, O. Bang, J. J. Rasmussen, and P. L. Christiansen, Opt. Lett. **29**, 286 (2004).
[23] Z. Xu, Y. V. Kartashov, and L. Torner, Optics Letters, **30**, 3171 (2005)
[24] S. Lopez-Aguayo *et. al.*, arXiv:nlin.PS/0512053 (2005).

- [25] V.I. Petviashvili and V.V. Yan'kov, Rev. Plasma Phys. Vol. 14, Ed. B.B. Kadomtsev, (Consultants Bureau, New York, 1989), pp 1-62.
- [26] Z.K. Yankauskas, Izv. Vyssh. Uchebn. Zaved. Radiofiz. **9**, 412 (1966) [Sov. Radiophys. **9**, 261 (1966)]
- [27] A.A. Kolokolov and A.I. Sykov, Zh. Prikl. Mekh. Tekh. Fiz., **4**, 55 (1975) [J. Appl. Mech. Tech. Phys. **4**, 519 (1975)]
- [28] J.M. Soto-Crespo, D.R. Heatley, E.M. Wright, N.N. Akhmediev Phys. Rev. A Vol. 44, (1991)
- [29] A. W. Snyder and D. J. Mitchell, Science 276, 1538 (1997)